# Performance Evaluation of Modified-Hybrid Radio Tomographic Imaging for Human Localization in Outdoor Environment

M.T.M Talib[1,2], M.H.F Rahiman[1,2*], R.A. Rahim[3], M.S.M. Abdullah [1,2]

[1]Faculty of Electrical Engineering Technology, Universiti Malaysia Perlis, Pauh Putra Campus, 02600 Arau, Perlis, Malaysia
[2*]Center of Excellence for Advanced Sensor Technology (CEASTech), Universiti Malaysia Perlis, 02600 Arau, Perlis, Malaysia
[3]School of Electrical Engineering, Faculty of Engineering, Universiti Teknologi Malaysia, 81310 Skudai, Johor, Malaysia

Corresponding author* email: hafiz@unimap.edu..my
Accepted 3 March 2021, available online 31 March 2021

**ABSTRACT**

The accuracy is the main factor in developing the localization system. However, due to the environmental noise and interference, the accuracy of localization has been affected. Since Device-free Localization has a multipath problem, thus Radio Frequency Tomography (RTI) has been introduced. This approach is used to localize the human position. This approach offers great potential in monitoring activities especially in perimeter surveillance application. Conventionally, RTI uses Linear Back Projection algorithm (LBP) to reconstruct the tomographic image. However, this algorithm suffers with the ill-posed problem caused by back-projection and the smearing effect due to the overlapping image. This leads to a low-quality tomographic image projection. To improve the quality tomographic image, several regularization approaches has been introduced by other researchers. However, because the target occupies only a small amount of space compared to the entire area monitored, the resulting image is blurred with noise. Therefore, this paper proposed a Modified Hybrid Radio Tomographic Imaging (HRTI-M). Through this proposed method, the area smeared on the RTI image has been reduced. Moreover, the average error of the reconstruction area has been able to be reduced from more than 3% to less than 1%.

**Keywords:** Radio Tomographic Imaging, Device free localization

## 1. Introduction

Numerous studies on the use of Device -free Localization Applications in human localization has been made. However, the disadvantage of existing DFL systems is the low localization accuracy because the significant variation of RSSI values is influenced by multipath interference and environmental noise [8]. Where RSSI -based localization estimates human location by measuring signal fluctuations due to human presence in the monitoring area [5]. In external localization, RSSI variations are introduced by environmental factors such as wind foliage, rainfall, and unstable external environment, which can affect the accuracy of localization [1].

The problem of localization accuracy can be solved by applying Radio Tomographic Imaging (RTI) technique. This technique gives excellent results on human localization because human location can be seen directly from tomographic images. Radio Frequency Tomography (RTI) is a technique used to localize the human position presented by Wilson and Patwari in 2009[1]. The cross-section image of a monitoring area is constructed by analyzing the receive signal strength (RSS) value and the attenuation of the radio frequency (RF) signal [1]. This approach offers great potential in monitoring activities such as perimeter surveillance monitoring, virtual fence for farm monitoring, and residential monitoring. Conventionally, RTI uses Linear Back Projection algorithm (LBP) to reconstruct the tomographic image. The fundamental of the LBP algorithm is the multiplication of the sensitivity matrix with the appropriate RSS value. However, the exact human location is still inaccurate because the projection image suffers from ill-posed problem and the smearing effect due to image overlap caused by the Linear Back Projection (LBP) algorithm [2]. These problem leads to low localization accuracy due to low-quality tomographic image reconstructed by LBP [2]. Several regularization approaches have been introduced to improve the quality tomographic image. There are three

standard regularization techniques proposed by researchers [1] to eliminate smear effects to improve tomographic image quality and improve localization accuracy namely Tikhonov single value deduction regularization (TSVD), total variation (TV), and compressing sensing (CS) algorithms. Among these three methods, Tikhonov regularization truncated singular value decomposition (TSVD) gives an acceptable localization accuracy. However, because the target occupies only a small amount of space compared to the entire area monitored, the resulting image is blurred with noise and interferes with target detection [2][3]. Therefore, this paper proposed a Modified Hybrid Radio Tomographic Imaging (HRTI-M) to reduce the impact of noise due to shadowing effect of measurement in the image reconstruction.

This paper is organized as follows: The model of HRTI-M and Gaussian model based on distance attenuation are introduced in section 2, the experimental design in Section 3 and the conclusions and discussion of the result has been highlighted in Section 4.

## 2. The Model of Radio Tomographic Imaging

The Radio Tomographic Imaging Model has been developed using a RF sensors network. The number of sensors nodes (N) has been arranged outside the monitoring area as shown in figure 1. The total number of measurements of RF sensor network can be obtained by M=N(N-1) by assuming the reciprocal of the measurement link are not equal due to differences in shadowing loss in each link caused by noise. From the observation of RSS attenuation, if the object is in the monitoring area, the RSS will be attenuated around -60dB to -80dB due to object obstruction. The shadowing loss of the sensor link ($Y_{loss}$) caused by object's obstruction can be determined as

.

$$\boldsymbol{Y_{loss} = P_{int} - P_{att}} \quad (1)$$

Where, $P_{int}$ is RSS measurement under initial condition (empty area) while $P_{att}$ is RSS measurement when object exist in the monitoring area, unit is dBm. The RF network has been modeled as a pixel grid with the size of m x n to obtain the attenuation images. Thus, the imaging area is divided into several small square areas which have the same size to represent the pixels. However, there is no limitation in determining the number of pixels used. if fewer pixels used, it will result in low-quality pictures while if a large number of pixels used, it will cause high computational time.

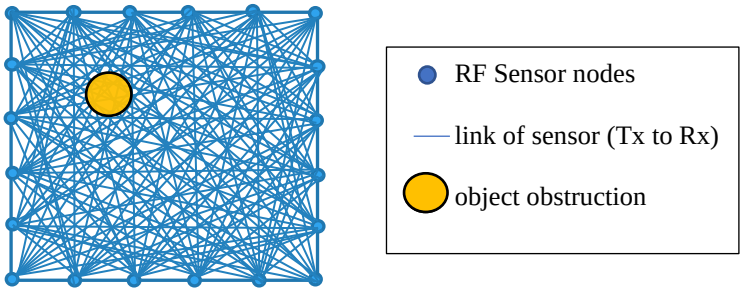


Figure. 1. Model of Radio Tomographic Imaging with RF sensor network

The pixel weight is determined based on the location of the pixel whether it is near or far from the line of sight (LOS) path. Typically, signal disruption models such as line models and elliptical models are used in determining how strong a link signal is interrupted by objects in a network. Through these models, the pixel will be weighted accordingly. Example of An RF link travel on the LOS path has been illustrated in figure 2.

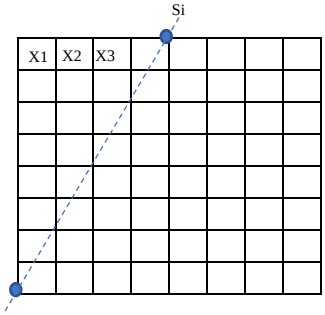


Figure. 2. A RF link travel on the LOS path

Thus, the attenuation (S) can be modelled as

$$S_i(t) = \sum_{j=1}^{N} \omega_{ij} x_j(t) \quad (2)$$

Where $x_j(t)$ is the attenuation when the signal passes through pixels j, $\omega_{ij}$ is the weight for each link and $S_i$ can be seen as a weighted sum $x_j$ [1]. Only pixels that are in the LOS path will be weighted while pixels that are not in the LOS path will be set to zero. Further, a sensitivity map is a sensitivity propagation plot obtained by calculating the radio frequency attenuation at the position of each receiver due to obstructions in the monitoring space.

### 2.1 **Image Reconstruction Algorithm**

Conventionally, the back-projection algorithm has been used to reconstruct the cross-section of image plane from the projection data. These projection data were obtained by measuring the attenuation of sensor values due to obstruction in the image field. Then, this projection data is projected back by multiplying it by the appropriate normal sensitivity map.

A plot of sensitivity distribution obtained by calculating the radio frequency attenuation at the position of each receiver due to obstacles in the monitoring area. To produce sensitivity distribution map, a model of measurement section has been developed. Therefore, the cross-section of the monitoring area is mapped into a 20 x 20 rectangular arrangement consisting of 400 pixels. Then, the image plane model is developed to 65 x 65 pixels. In this experiment, the Gaussian model has been used to determine the weightage of the pixel.

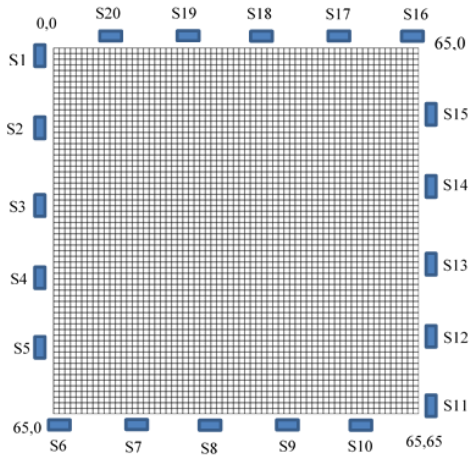


Figure. 3. Image plane of 65 x 65 pixels tomogram

### 2.2 **Gaussian Model**

In this research, a new signal interference model known as the Gaussian model has been used as an alternative method to the elliptical model by assuming that the propagation of environmental noise including multipath interference is corresponding to a normal or Gaussian distribution. To provide the pixel weightage, the general gaussian equation expressed in equation (3) has been referred where α is the peak of the curve, μ is center of the peak and σ is the standard deviation that control the peak' width. This Gaussian Function has been illustrated in figure 4. Through this model, the pixel weight is given depending on the distance of the pixels from the LOS path as expressed in equation (4). Where, $d_l$ is the length of the LOS path between two sensor nodes and $d_{l,p}$ is the sum of the distance from the sensor nodes to the center of the pixel. If the pixel lies on the LOS path, it will have the highest weight while the pixel farthest from the LOS will get the lowest weight as illustrated in figure 5.

$$f(x) = \alpha e^{-(\frac{x-\mu)^2}{2\sigma^2}} \quad (3)$$

$$\omega_{l,p} = e^{-(\frac{d_{l,p}-d_l)^2}{2\sigma^2}} \quad (4)$$

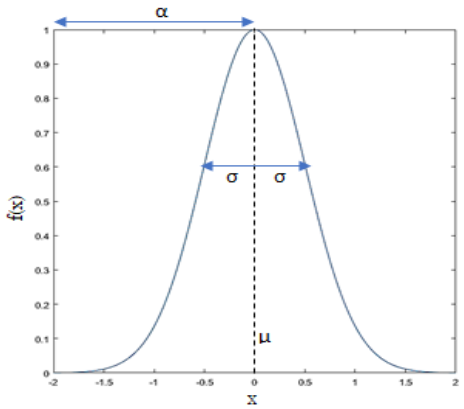


Figure. 4. Gaussian function with α=1, μ=0, σ=0.5

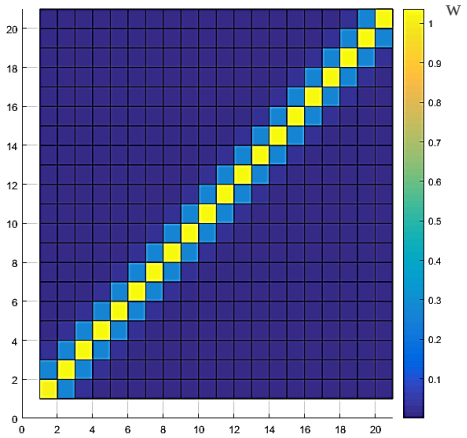


Figure. 5. Gaussian function with α=1, μ=0, σ=0.5

Meanwhile, a tomographic image of human location projected by the Gaussian model is shown in figure 6. Referring to this tomographic image, the red color in this image represent the high permittivity area which contains the information of the human location.

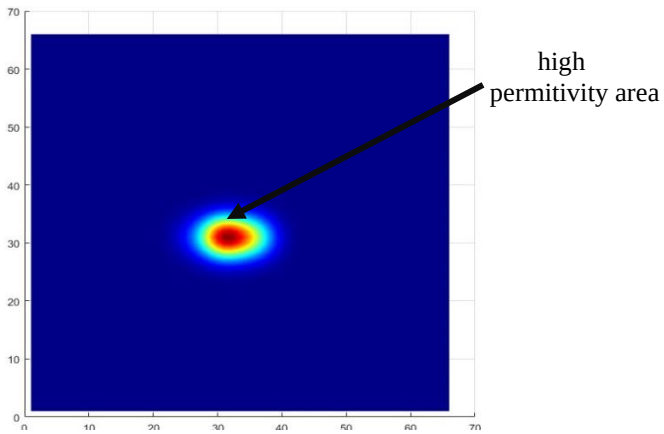


Figure. 6. Tomographic image of human location projected by Gaussian model

### 2.3 Modified Hybrid RTI Approach (HRTI-M)

To reduce the smeared area on the RTI image, another image reconstruction technique named as Modified Hybrid Radio Tomographic Imaging (HRTI-M) has been introduced. This HRTI-M is obtained by multiplying each sensor value with its sensitivity map projected by Gaussian model. However, in this HRTI-M approach, Threshold Sensor Value (TSV) method has been applied. If the normalized sensor value ( $\bar{N}_{Tx,Rx}$ ) is more than or equal to threshold value Nr, then its sensitivity map is set to the maximum pixel value (i.e., 255). But, if the normalized sensor value is less than threshold value, it is set to minimum pixel value which is zero. This threshold value refers to the normal ratio of RF attenuation obstructed by the human body. In this experiment, a small person was used. From the observation, it is found that the normalized attenuation ratio is 0.2. However, the threshold value depends on the human size. If the size of the human body is bigger, then the attenuation is higher. Thus, the threshold value will exceed 0.2. This threshold value is needed to filter up the highly effected link data and remove the low effected link data. Mathematically, The HRTI-M model is expressed as

$$A_{HRTI-M}(i,j) = \sum_{Tx=1}^{20} \sum_{Rx=1}^{20} \bar{N}_{Tx,Rx} \times \omega_{Tx,Rx}(i,j) \tag{5}$$

As mentioned above, the value of $\bar{N}_{Tx,Rx}$must fulfill specific conditions as follows

$$\bar{N}_{Tx,Rx} = \begin{cases} 255 & if\ N_{(Tx,Rx)} \geq N_r \\ 0 & if\ N_{(Tx,Rx)} < N_r \end{cases} \tag{6}$$

Where, $\omega_{Tx,Rx}(i,j)$ is a sensitivity map based on the gaussian weight model. However, to applied this HRTI-M model, the weight formula has been modified as stated in (7). This modification was made to minimize the smear effect on the RTI image by adjusting the standard deviation (σ) of the gaussian weight model. This approach can be mathematically expressed as follows

$$\omega_{Tx,Rx}(i,j) = e^{-\left(\frac{d_{l,p}-d_l)^2}{2(\frac{1}{2}\sigma^2)}\right)} \tag{7}$$

Where, $\mathbf{d_l}$ is the length of the sensor nodes link and $\mathbf{d_{l,p}}$ is the total distance from the center of the pixel to the end of link (sensor nodes). Figure 7 illustrates the tomographic image of human location projected by HRTI-M.

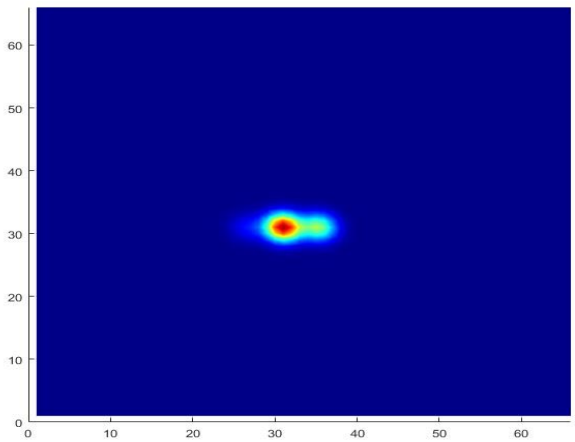


Figure. 7. Tomographic image of human location projected by HRTI-M

## 3. Experimental Design

An experiment has been designed to gather information about the human body attenuation. The information about RSS data for both stage (calibration and attenuation) help in designing the system model. By taking the average diameter of the human body is 50cm, monitoring area of 5m x 5m has been divided into nine grids to represent a zone, as shown in figure 8 (a). Hence, each zone can contain up to five positions of human. Figure 8 (b) shows the affected pair of the link, which gives high attenuated data. Where the area in the circle contains high attenuated data, which presents the human position in the monitoring area. Figure 9 shows the experimental setup for monitoring area of 5m x 5m. The RSS value of the baseline dataset collected under the calibration period (without the presence of human).

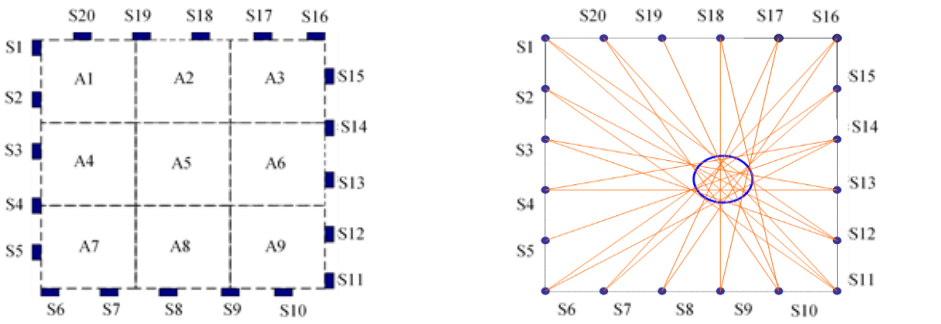


(a) 9 zone of monitoring area (b) Effected pair of links due to human presence

Figure. 8. Experimental design for human localization

Figure. 9. Sensor array follow experimental design

A square monitoring area as shown in figure 10 (a) with dimensions of 5 meters x 5 meters was prepared for the experiment. Then, these monitoring areas were arranged with 20 units of RF sensors where the distance of each was one meter. Referring to the theoretical of RF network propagation, as the distance between transmitter and receiver increase, the local average of the received signal power decreases gradually. If the gap between sensors is too closed, the number of sensors used will increase. This will result in high time consumption to collect the data. However, if the gap between the sensors is too large, it will cause an increase in the size of the monitoring area to accommodate 20 sensors. If this happen, the distance of transmitter to receiver will be increase too. On the other side, if we want to maintain the size of the monitoring area at 5mx5m, the use of sensors should be reduced. this will affect the quality of the image that will be produced. The experiment was conducted in two situations; (i) in the empty condition and (ii) with existence of human. Further, humans are in a static position at each location mark while the measurement is performed. Figure 10 (b) shows a single scan transmitter to several receiver sensors. Where, the red line is the affected link because human presence provides attenuation data. These observations were made to observe the effect of the human body on RSSI measurements. From these observations, it is known that the RSS measurement range during the calibration period (empty condition) is around -40 to -60 dBm. Meanwhile, the RSS measurement range for human presence in the monitoring area is around -61 dBm to -80 dBm.

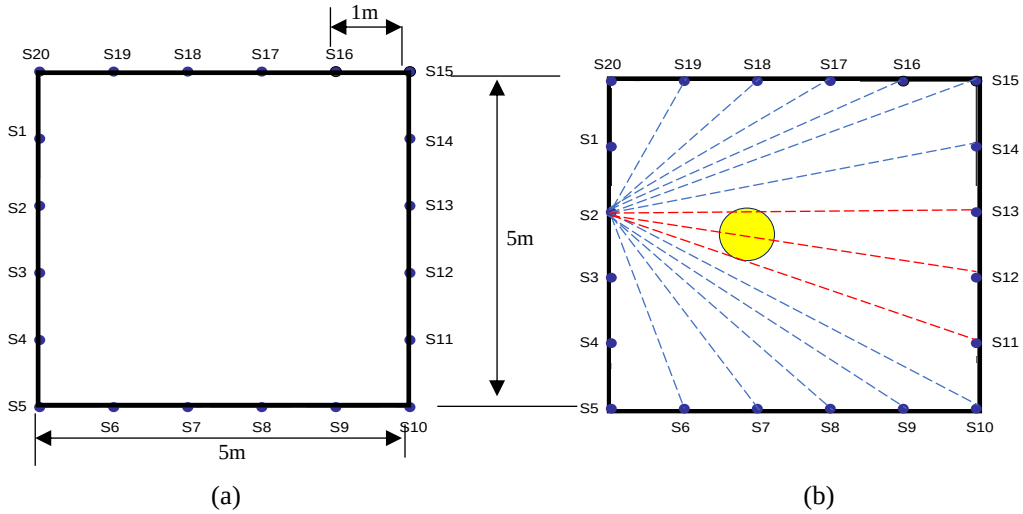


Figure. 10. (a) detection areas with Wi-Fi sensor's arrangement (b) measurement projection for single scanning transmitter to multiple receivers

In this experiment, each sensor acts as a transceiver. For example, in a single scan, sensor (S2) sends a signal while another sensor will receive the signal sent by S2. The scanning process will be repeated until all sensors send a signal. The attenuation of radio signal strength ($Att_{(Tx,Rx)}$) due to human presence can be obtained as

$$Att_{(Tx,Rx)} = M_{ref-} M_{(Tx,Rx)} \tag{8}$$

Where $M_{(Tx,Rx)}$ is attenuation data for the current human position, and $M_{ref}$ is reference data during an empty condition (calibration). The link measurements are considered to be simultaneous and all the parameters in (8) are arranged in the matrices form.

## 4. Result and discussion

### 4.1 Comparison of the performance of image reconstruction algorithms

### 4.2 Performance analysis of image reconstruction method

Performance evaluations for the Gaussian and HRTI-M approaches were performed. This evaluation is made to find out the effectiveness of the proposed approach. Therefore, a comparison of the RTI image projected by Gaussian and HRTI-M has been illustrated in Table 1. From these results, the image quality produced by Gaussian is still low due to the large smeared area on the image which may cause localization in the wrong place. It is difficult to get the exact human location with high accuracy because of the smeared area. On the other hand, HRTI-M has produced a better quality of reconstructed image compare to the image projected by Gaussian. Through this method, the smeared area on the image has been reduced. This approach was also tested when two humans were in the monitoring area as shown in Table 1 (referring to sample 4). Typically, the problem faced by conventional method like Linear Back Projection and Gaussian is that reconstructed images of two closer human positions tend to merge together. Thus, by introducing the HRTI-M method, the problem of merging 2 nearby human locations can be solved.

**Table 1.** Error of reconstructed image for HRTI-M

| PHANTOM | Gaussian | HRTI-M |
|---|---|---|
| 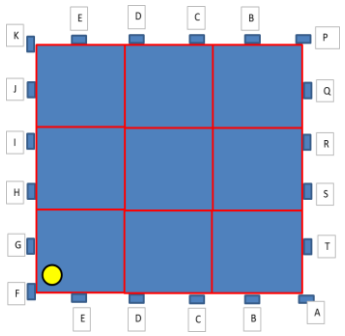 Sample 1 | 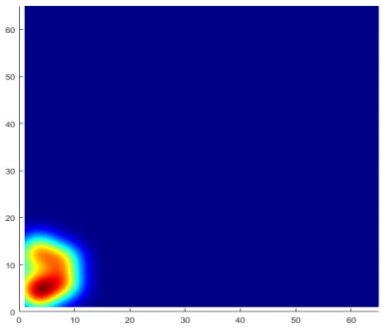 | 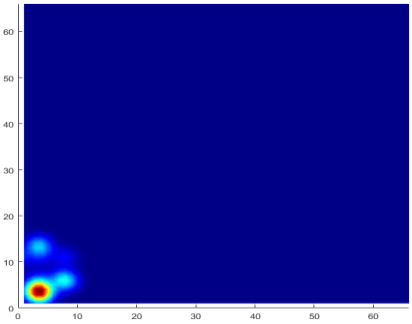 |
| 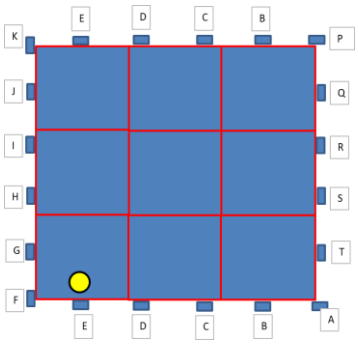 Sample 2 | 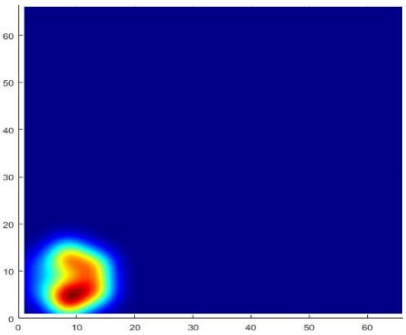 | 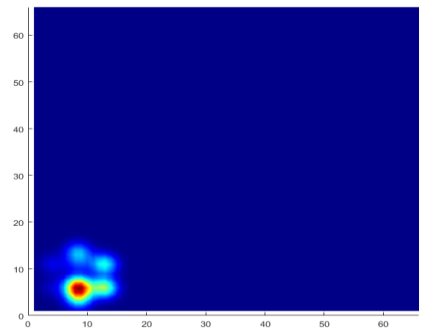 |
| 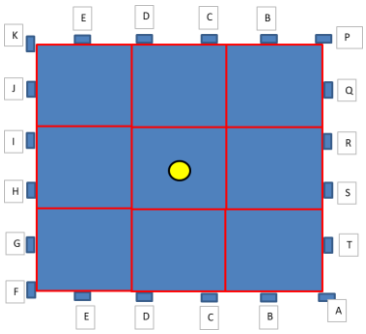 Sample 3 | 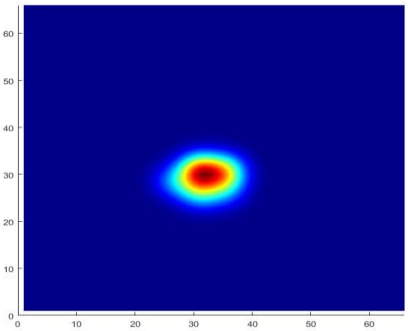 | 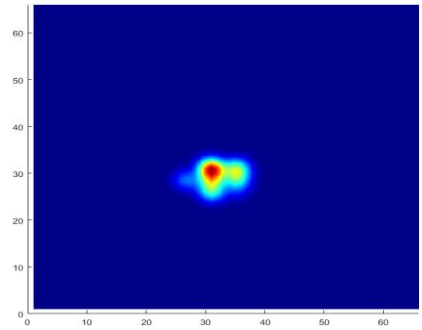 |
| 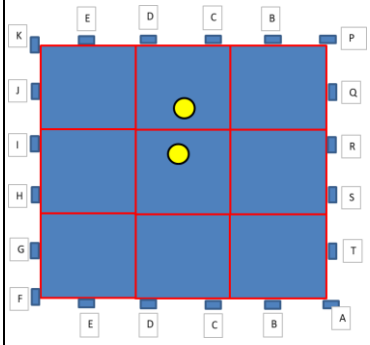 Sample4 | 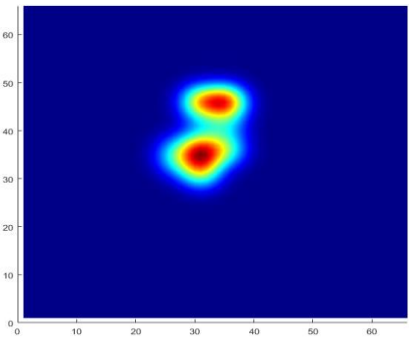 | 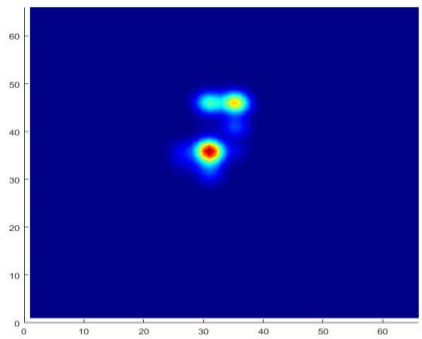 |

The quality of tomographic imaging can be assessed by comparing image of reconstructed physical models with actual cross-sections [5]. The comparisons are made based on reconstructed image with standard image corresponding to the cross section of the physical model [6][7]. Where, the standard image is an array of M pixels defining the standard (test) model by the color level of each pixel. In this analysis, the area error percentage (AE%) was calculated based on colored pixels which representing the permittivity levels. The summation of colored pixel then will be divided by the total number of pixels of an image. Table 2 illustrates the result of AE% for comparison. The area error percentage of HRTI-M is lower than 1% while the area error percentage of Gaussian is slightly higher for all tested samples. Thus, known that the performance of HRTI-M is better compared to Gaussian. The percentage of area errors was plotted graphically for easy reference.

**Table 2.** Error of reconstructed image for proposed algorithm

| Sample Location(s) | Gaussian AE(%) | HRTI-M AE(%) | Improvement (%) |
|---|---|---|---|
| 1 | 3.36 | 0.42 | 2.94 |
| 2 | 4.35 | 0.75 | 3.6 |
| 3 | 1.13 | 0.21 | 0.92 |
| 4 | 4.16 | 0.68 | 3.48 |

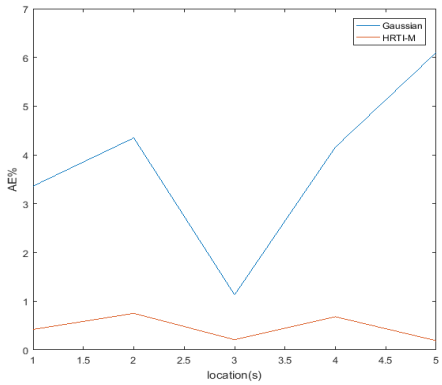


Figure. 11. Area error analysis graph

Furthermore, accuracy is a main concern to evaluate the effectiveness of the method. Since area errors have been reduced, localization accuracy can be improved. As area errors have been reduced, localization accuracy can be improved. Table 3 shows the accuracy obtain for both approaches. Through this comparison, it can be seen that the accuracy of HRTI-M exceeds 98% for all the given samples where the percentage is slightly higher compared to Gaussian.

**Table 3.** Accuracy of localization projected by proposed algorithm

| Sample Location(s) | Gaussian (%) | HRTI (%) |
|---|---|---|
| 1 | 96.14 | 99.08 |
| 2 | 95.15 | 98.75 |
| 3 | 98.37 | 99.29 |
| 4 | 95.34 | 98.82 |

To further strengthen these findings, further analysis was conducted using Structural Similarity Index Measure (MSSIM), Mean Squared Error (MSE), and Peak Signal to Noise Ratio (PSNR). These evaluations are necessary to evaluate the performance of the proposed method. All the results of the performance analysis have been compiled in Table 4. Referring to the analysis results, the performance of HRTI-M is better when compared with Gaussian for all the analyzes performed. The reduction of the smeared area performed by HRTI-M has helped in minimizing the measurement of the peak area (which was our focal point in this study). Moreover, SSIM analysis showed that the equation results were improved by about 8% to 96% compared to Gaussian. This means the image constructed by HRTI-M is closer to the reference model. Meanwhile, the MSE analysis tested on the RTI image also showed that the

HRTI-M showed good performance compared to Gaussian. Where the MSE has been improved around 8% to 32% using this proposed approach. The same is true for PSNR evaluations for HRTI-M performance. It is seen to be slightly higher than the Gaussian. Theoretically, it is known that the higher the PSNR, the better the quality of the reconstructed image [8]. From all these analyzes, it is known that HRTI-M performance is better and can be used to improve the quality of reconstructed images.

**Table 4.** Performance analysis of Gaussian and HRTI-M approach

| Algorithm(s) | Gaussian | | | HRTI-M | | | Improvement (%) | | |
|---|---|---|---|---|---|---|---|---|---|
| Sample(s) | MSSIM | MSE | PNSR | MSSIM | MSE | PNSR | MSSIM | MSE | PNSR |
| 1 | 0.033 | 650.039 | 20.001 | 0.071 | 544.133 | 20.774 | 36.268 | 8.869 | 1.894 |
| 2 | 0.025 | 711.973 | 19.606 | 0.030 | 654.935 | 19.969 | 8.633 | 4.173 | 0.916 |
| 3 | 0.018 | 796.541 | 19.119 | 0.938 | 460.329 | 21.500 | 96.154 | 26.750 | 5.863 |
| 4 (2 persons) | 0.006 | 1589.936 | 16.117 | 0.066 | 811.124 | 19.040 | 83.079 | 32.436 | 8.314 |

## 5. Conclusion

This paper presents HRTI-M as a new image reconstruction algorithm. Comparisons made between HRTI-M and Gaussian prove that HRTI-M performance is better. Where the accuracy of HRTI-M exceeds 98%. Proved that, the reduction of the area smeared on the tomographic image has improved the localization accuracy. Thus, future work will be focused on Experiment the HRTI-M approach in real-time application.

## Acknowledgment

The authors would like to thank the Ministry of Education Malaysia for their sponsorship and financial support. Acknowledgments and thanks also to the Japan Science and Technology Agency, Yamanashi University, and the Center of Excellence for Advanced Sensor Technology (CEASTech), Universiti Malaysia Perlis for offering research collaboration opportunities under the Sakura Exchange Program in Science. Finally, many thanks to my supervisor and all the postgraduate members under him for their help and support in this project.

## References

[1] Wilson, J., Patwari, N., & Vasquez, F. G. (2009, June). Regularization methods for radio tomographic imaging. In *2009 Virginia Tech Symposium on Wireless Personal Communications*.

[2] Xu, S., Liu, H., Gao, F., & Wang, Z. (2019). Compressive sensing based radio tomographic imaging with spatial diversity. *Sensors*, *19*(3), 439.

[3] Wang, Q., Yiğitler, H., Jäntti, R., & Huang, X. (2015). Localizing multiple objects using radio tomographic imaging technology. *IEEE Transactions on Vehicular Technology*, *65*(5), 3641–3656.

[4] van der Meij, T. (2017, September). Mobile Radio Tomography: Agent-Based Imaging. In *BNAIC 2016: Artificial Intelligence: 28th Benelux Conference on Artificial Intelligence, Amsterdam, The Netherlands, November 10-11, 2016, Revised Selected Papers*, *765*, 63. Springer.

[5] Ortiz-Alemán, C., Martin, R., & Gamio, J. C. (2004). Reconstruction of permittivity images from capacitance tomography data by using very fast simulated annealing. *Measurement Science and Technology*, *15*(7), 1382.

[6] Xie, C. G., Huang, S. M., Lenn, C. P., Stott, A. L., & Beck, M. S. (1994). Experimental evaluation of capacitance tomographic flow imaging systems using physical models. *IEE Proceedings-Circuits, Devices and Systems*, *141*(5), 357–368.

[7] Rahiman, M. H. F., Rahim, R. A., Rahim, H. A., Muji, S. Z. M., & Mohamad, E. J. (2012). Ultrasonic tomography-image reconstruction algorithms. *International Journal of Innovative Computing, Information and Control*, *8*(1), 527–538.

[8] Hore, A., & Ziou, D. (2010, August). Image quality metrics: PSNR vs. SSIM. In *2010 20th international conference on pattern recognition*, 2366–2369. IEEE.